Experience in the Development of the Sine-Wave Filter for High-Power Variable Voltage Variable Frequency Drive with Medium Voltage Induction Motor

MIKHAIL PUSTOVETOV
Department of Electrical and Electronics Engineering,
Don State Technical University,
344000, Rostov region, Rostov-on-Don, Gagarin sq., 1
RUSSIA

Abstract: - The relevance of the work reflects the increased use in practice of variable frequency electric drive additional options, which include sine-wave filter. The main aim of the study: is to develop guidelines for choosing the parameters of the sine-wave filters and the correct selection of the elements in the current; consider the phenomena occurring when the capacity is connected to terminals of the load with an induction motor, such as: reactive power compensation and overcompensation, self-excitation. The methods used in the study: test on a real process plant; and computer simulation of an electromechanical system with a semiconductor converter based on a combination of circuit and operational principles for preparing the model. The results: some of the results of experience in the design and testing of the sine-wave filter for high-power variable voltage variable frequency drive with medium voltage induction motor with scalar control are described. The comparative results of the computer simulation of processes at different sets of the sine-wave filter and converter parameters are presented. Some recommendations for sine-wave filter design are suggested.

Key-Words: - frequency converter, pulse-width modulation of voltage, sine-wave filter, induction motor, capacitance, reactive power, self-excitation, current.

Received: May 8, 2024. Revised: September 11, 2024. Accepted: November 10, 2024. Published: December 5, 2024.

1 Introduction

In order to smooth the pulse edges of the pulse-width modulated (PWM) voltage supplied to the terminals of induction motors (IM) from frequency converters (FCs), output filters are used between the FC and the IM, [1], [2], [3], [4], [5], [6], [7], [8], [9], [10]. The negative impact of PWM voltage on electrical equipment in the absence of an output filter is expressed in: high-frequency noise of the IM [11], [12], [13], increasing level of electromagnetic interference [14], electro corrosion and destruction of motor bearings and driven mechanisms [15], [16], [17], [18], [19], [20], gradual degradation of electrical insulation [21], [22], [23], accompanied by intense generation of ozone, which is harmful to personnel, [24], [25].

A solution to the problem is to use a sine-wave filter (SF) (Figure 1). It brings the shape of the output voltage of the inverter as close as possible to a sinusoid, thereby minimizing the value of the total harmonic distortion (THD) factor of the phase-to-phase voltage k_V [26] and THD of the current I_2 - k_{I2} [26], [27].

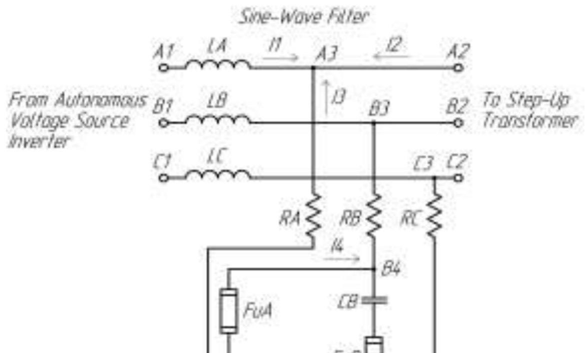

Fig. 1: Electrical circuit diagram of SF (alternatively, fuses can be connected in series with the damping resistors RA, RB and RC)

It is advisable, in any case for the frequency of the fundamental harmonic of the output voltage of the inverter $f_1 = 50$ Hz, to require that the output voltage after the SF correspond to the grid voltage: the THD of the supply voltage (including all harmonics up to the order 40) shall be less than or equal to 8 %, [26], (k_V no more than 12% at

380 V RMS grid's rated voltage in accordance with Russian State Standard, [28]). The complexity of choosing SF parameters increases at the carrier frequency of the PWM $f_{car} < 2$ kHz - a significant capacitance is obtained (over 1000 μF). This circumstance forces us to pay attention to possible features, as well as the positive and negative effects of connecting a capacitance to the terminals of a load containing an IM. Let's look at a few specific provisions below.

2 Problems Formulation

1. The current through the SF capacitors increases as the load on the IM shaft decreases.
2. In addition to the function of the SF element, the capacitance can also perform the function of compensating the reactive power of the IM and the step-up transformer.
3. A significant capacitance will most likely be composed of several parallel-connected capacitors, possibly of different ratings and with different characteristics.
4. The SF capacitance can form resonant circuits with inductances in various branches of the circuit diagram.
5. If the voltage at the inverter output fails, the SF capacitance, remaining connected to the load circuit containing the IM, can lead to self-excitation of the IM, accompanied by significant currents and voltages.

Fig. 2: An electric drive of the pump of type 14D6 (right side of the photo) as a part of WPS based on a four-pole IM (left side of the photo) with a rated phase-to-phase voltage of 6 kV and a rated shaft power of $P_{2rated} = 630$ kW

Further explanations will be given using the example of a specific technological installation - an electric drive of the pump of type 14D6 as a part of a water pumping station (WPS), [29], based on a four-pole IM with a rated phase-to-phase voltage of 6 kV and a rated shaft power of $P_{2rated} = 630$ kW (Figure 2). The calculated parameters of the IM equivalent circuit are published in [30]. At the rated operating mode of the pump, the load of IM is $0.73 \cdot P_{2rated}$. The IM is powered using a two-transformer circuit [9], [31] (Figure 3) from the FC of type Vesper EI-7009-1000N (six-pulse diode rectifier plus two-level voltage source inverter, [32]), which has a range of PWM carrier frequencies $f_{car} = 1...2.5$ kHz and the highest permissible RMS output current of phase at continuous running duty (operating mode S1), [33] $I_{1\ \lim} = 1600$ A. The inductive branch of the SF in each phase is represented by a pair of parallel-connected current-limiting reactors RTST-820-0.0505 U3 (Figure 4). The resistance of one reactor is 1.65 mOhm. In those cases where the absence is not specified, the presence in the diagram is implied according to Figure 1 in the power lines of the capacitive part of the SF damping resistors RA, RB, and RC with a rated value of 0.013468 Ohm.

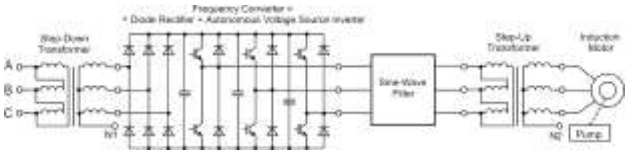

Fig. 3: The IM is powered using a two-transformer circuit

During commissioning work with a capacitance of the SF of 8360 μF per phase and absence in the circuit in Figure 1 resistors RA, RB, and RC at a frequency f_1 of about 12 Hz, about 27 Hz and especially 41.9-42 Hz there was a noticeable increase in the current at the output of the inverter. Around $f_1 = 42$ Hz, the inverter switched off due to a "short circuit at the inverter output." An increase in current, current surges and fluctuations in current magnitude were visible in a fairly wide band of adjacent frequencies (bandwidth 7 Hz or more). Therefore, using the frequency hopping IF function will not be effective. In addition, the current resonance frequency band may fall within the range used for the operation and control of the drive. By sequentially removing fuses on 1000 μF capacitors symmetrically across the phases of the SF, with a capacity of 3360 μF per phase, it was possible to achieve a non-stop start of the drive with a frequency increase rate from 0 to 50 Hz in 90 s with the pump running on a closed gate valve, [34] (that is, with a reduced load). However, current swings with a frequency of the order of several hertz continued to be present, including at $f_1 = 50$ Hz. When the capacity of the SF phase was reduced to 1360 μF, the fuse links burned out during the startup of the IM without load.

Fig. 4: Pair of 3-phase current-limiting reactors RTST-820-0.0505 U3

3 Problems Solution

The first position is illustrated in Figure 5, which shows the calculated dependences of the SF currents (determined by the power released at the active resistance when current is passed through it) according to the diagram in Figure 1 at $f_1 = 50$ Hz. When approximating the current graph $I_4 = f(P_2)$ of curve 6 in Figure 5 by the expression y = 0.0000000001x4 - 0.0000003028x3 + 0.0002864698x2 - 0.1487129951x + 375.429507481 the coefficient of determination, [35], [36] is $R^2 = 0.9999999995$. On the contrary, the current through the SF inductance increases with increasing load on the IM shaft. All dependencies shown in Figure 5, Figure 6, Figure 7, Figure 8, Figure 9, Figure 10 and Figure 11, were obtained as a result of computer simulation by means of OrCAD, [37], [38], [39] of steady-state operating modes of the electric drive.

When constructing the simulation model of an electric drive, the following were used: approaches and relationships for calculating SF parameters given in [40], [41], [42], [43], [44], [45], [46], a mathematical model of a three-phase IM, [47], [48], [49], [50] and a three-phase transformer [51], a computer model of autonomous voltage source inverter, [40], [52].

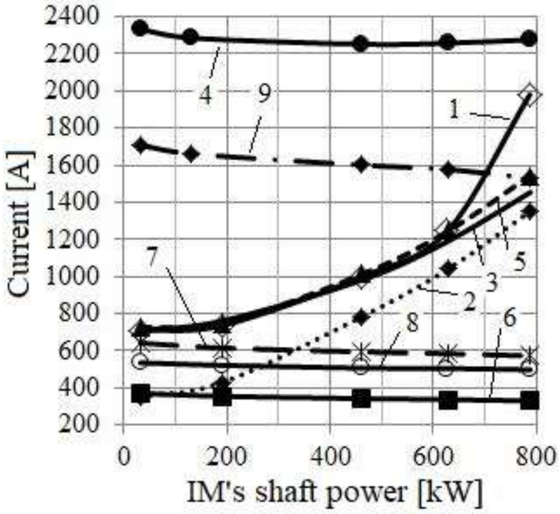

Fig. 5: Calculated currents of the SF: 1 - $I_1 = I_2$ without capacitors at $f_{car} = 2.5$ kHz; 2 - I_1 with an SF capacity of 2200 μF per phase, $f_{car} = 2.5$ kHz; 3 - I_1 at 2200 μF, $f_{car} = 1$ kHz; 4 - I_1 at 8360 μF, $f_{car} = 2.5$ kHz and the absence of damping resistors; 5 - I_2 at 2200 μF, $f_{car} = 2.5$ kHz (the I_2 curves for other cases are very close to the one shown); 6 - I_4 at 2200 μF, $f_{car} = 2.5$ kHz; 7 - I_3 at 2200 μF, $f_{car} = 2.5$ kHz; 8 - I_4 at 2200 μF, $f_{car} = 1$ kHz; 9 - I_4 at 8360 μF, $f_{car} = 2.5$ kHz and no damping resistors

If it is necessary to determine the RMS value of the current in a transient process, for example, during frequency acceleration of the IM, you should select the current curve for harmonic analysis over a time interval equal to the period of the fundamental harmonic. Having squared the current curve over a period, we will then perform its harmonic analysis. The resulting constant component will correspond to the power that will be dissipated at the resistance of 1 Ohm when the current in question flows through it. That is, the square root of the resulting constant component is the RMS value of the current, taking into account all harmonics over the selected time interval.

The second position is also confirmed in Figure 5: with a capacitance per phase of the SF of 2200 μF, the current at the output of the SF (load current) exceeds the current at the input of the SF (consumed from the inverter) due to the compensation of the reactive power of the load with the SF capacitors. The phenomenon is known for capacitive reactive power compensators IM, [53], [54], [55], [56], [57].

From Figure 6 it can be seen that with increasing capacity SF for I_4 decreases k_{I4}. All other things being equal, this occurs with an increase in capacitance due to an increase in the proportion of the fundamental harmonic in the harmonic spectrum of the current I_4, at which reactive power compensation occurs.

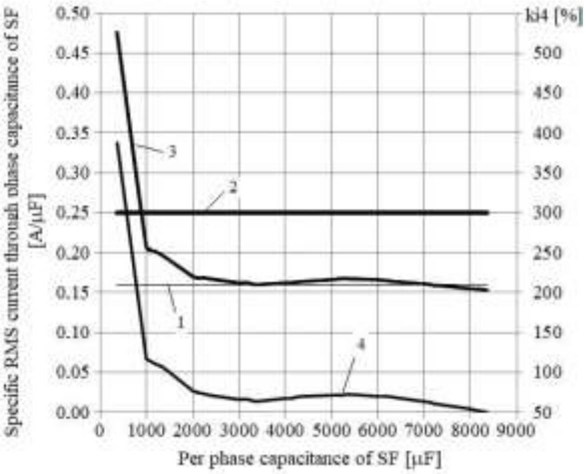

Fig. 6: Calculated specific RMS current through the SF capacitance and the THD of the I_4 current at $f_1 = 50$ Hz and load on the IM shaft equal to $0.05 \cdot P_{2rated}$. The curves were obtained with connected damping resistors. In their absence, the specific RMS current through the capacitance is 1.3–1.4 times higher. 1 – permissible specific RMS current 0.16 A/μF for capacitors with a capacity of 1000 μF; 2 – permissible specific RMS current 0.25 A/μF for capacitors with a capacity of 160 μF and 200 μF; 3 – calculated specific RMS current through the SF capacitance; 4 - k_{I4}

However, from the same Figure 5 it can be seen that with a capacitance per SF phase of 8360 μF, the output current of the inverter significantly exceeds the load current and depends little on changes in the power on the IM shaft. At the same time, the I_2 curve is close to the case with a SF capacitance of 2200 μF. The calculation showed that to fully compensate for the reactive power of the load when the IM is operating in the rated mode, a SF capacitance of 2564 μF is sufficient. That is, “overcompensation” of the reactive power of the load by overestimating the capacity of the SF leads to a noticeable I_1 increase. When simulating with a SF capacitance of 8360 μF at a low load on the IM shaft without damping resistances for $f_1 = 40$ Hz and $f_{car} = 2.5$ kHz, the specific current through the capacitance was 0.101 A/μF, while at $f_1 = 45$ Hz it was already 0.181 A/μF. Accordingly, the RMS values of the output current of the inverter at continuous duty is 972.3 A and 1995.6 A. Thus, around $f_1 = 42$ Hz there is a sharp increase of I_4 and the output current of the inverter exceeds the value $I_{1\,\lim} = 1600$ A with a further increase, to which the inverter responds by shutting down on the basis of “short circuit at the output”. The multiple I_1 increase in the low load mode of IM with an SF capacitance of 8360 μF compared to the case of no capacitance has been confirmed by tests.

The third point is illustrated by a specific example: the SF phase capacitance of 8360 μF, calculated from the operating condition at $f_{car} = 1$ kHz, was practically obtained by combining capacitors with ratings of 1000 μF, 200 μF, and 160 μF. Each capacitor is protected by a fuse. The maximum RMS values of long-term current are 40 A for 160 μF, 50 A for 200 μF and 160 A for 1000 μF. Accordingly, the long-term permissible specific RMS current per unit of capacitance is 0.25 A/μF for the lower ratings of capacitors, and 0.16 A/μF for the higher ratings. Thus, if we connect as shown in Figure 5, per phase SF 2200 μF, then based on the sum of currents through the fuses, 370 A per phase is permissible for a long time, and on this basis, it should be according to Figure 5 and Figure 7, expect that at $f_1 = 50$ Hz, $f_{car} = 2.5$ kHz and a load on the IM shaft of more than $0.05 \cdot P_{2rated}$, the capacitors will not be overloaded by current in long-term operation. But the current through parallel-connected capacitors is distributed in direct proportion to their capacitances. It follows that the admissibility of loading capacitors with current in the presence of parallel-connected high and low ratings should be assessed by a value of 0.16 A/μF.

From Figure 7 it can be seen that only when the power on the IM shaft is above $0.4 \cdot P_{2rated}$ that we have an acceptable current load on the capacitors at continuous duty. Otherwise, since the calculated specific RMS capacitance current exceeds the permissible value of 0.16 A/μF slightly, the protection (fuse links) will be triggered, first of all, by capacitors rated 1000 μF due to overload current (due to overheating at continuous duty). This was observed during the commissioning of the SF on the WPS, when a continuous duty was tested at

$f_1 = 50$ Hz and no load condition on the IM shaft and capacitors on the SF phase of 2200 µF and 2000 µF (fuses' elements melting within 10 - 15 minutes) or 1000 µF (fuses' elements melting within 5 minutes).

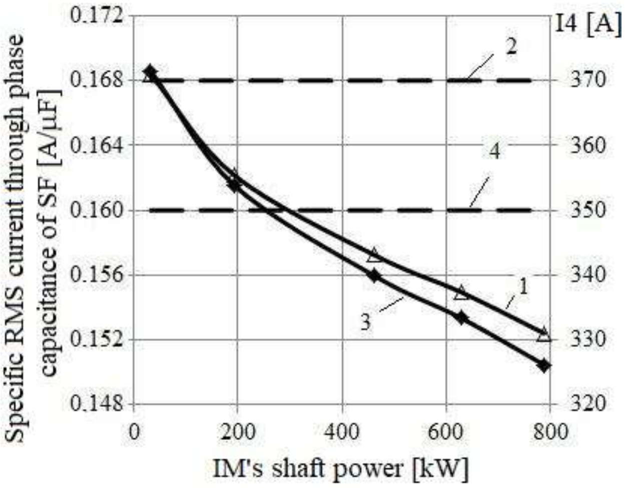

Fig. 7: I_4 and the specific RMS capacitance current as a function of the power on the IM shaft for the case of capacitance in the SF phase of 2200 µF, $f_1 = 50$ Hz and $f_{car} = 2.5$ kHz: 1 - ; 2 – highest permissible RMS current at continuous duty $I_{4\,\mathrm{lim}} = 370$ A; 3 – specific RMS current through capacitance at continuous duty; 4 - highest (equal to 0.16 A/µF) permissible specific RMS current through capacitance at continuous duty

From Figure 6 it follows that with a shaft power of IM equal to $0.05 \cdot P_{2rated}$, $f_1 = 50$ Hz and $f_{car} = 2.5$ kHz, we have a permissible load of capacitors by current in a continuous duty with a capacitance in the SF phase of at least 7160 µF, if damping resistors are connected.

With the adopted current-limiting reactors in the inductive part of the IF output filter, it can perform the functions of the SF with a capacitance value per phase of at least 360 µF at $f_{car} = 2.5$ kHz. To create a capacitance of 360 µF, only capacitors of 160 µF and 200 µF ratings with a large permissible specific current are used. But in this case, the value of the calculated specific RMS current is almost twice as high as 0.25 A/µF (Figure 6). You should expect rapid burnout of the fuses protecting the capacitors due to inrush current such as short circuit current. When carrying out commissioning work on the SF with a capacity of 360 µF per phase, the melting of the fuses' elements occurred already during the frequency start-up of an unloaded IM at $f_1 = 20...25$ Hz (approximately 40 s after the start of the frequency acceleration of the IM). The fuses' bodies didn't even have time to heat up.

Figure 8 shows the calculated graphs of the specific RMS currents of the SF capacitances at continuous duty as a function of the frequency of the output voltage of the inverter for three values of capacitance in the SF phase at low loads on the IM shaft in case of the presence of damping resistors RA, RB and RC in the capacitive part of the SF.

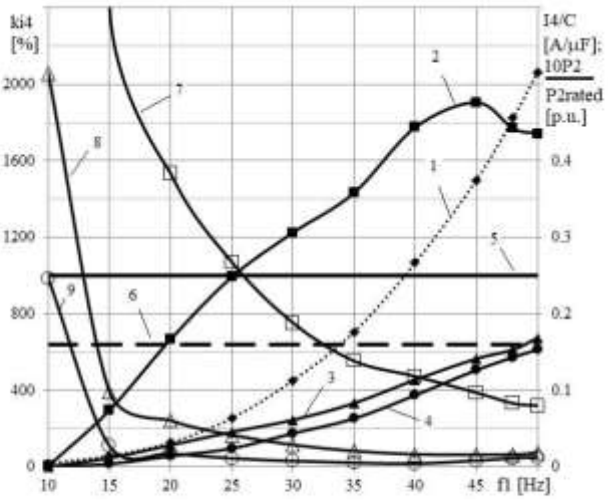

Fig. 8: Specific RMS current at continuous duty through capacitance and k_{I4} as a function of the frequency of the output voltage of the inverter for cases of capacitance in the SF phase of 360 µF, 2200 µF and 8360 µF at $f_{car} = 2.5$ kHz, low loads on the IM shaft and connected damping resistors: 1 - $10P_2 / P_{2rated}$ (ratio of power on the IM shaft to rated); 2 - specific RMS current at 360 µF; 3 - specific RMS current at 2200 µF; 4 - specific RMS current at 8360 µF; 5 – highest permissible specific RMS current of capacitors with ratings of 160 µF and 200 µF at continuous duty; 6 – highest permissible specific RMS current of capacitors rated 1000 µF at continuous duty; 7, 8, 9 - k_{I4} with a capacity of 360 µF, 2200 µF and 8360 µF, respectively

From Figure 6 it can be seen that with a capacitance of 8360 µF, the specific RMS current through capacitance is below the highest permissible value at continuous duty in the entire range of f_1. At 2200 µF the specific RMS current through capacitance is below the highest permissible value up to $f_1 = 49$ Hz, and at 360 µF - only up to the frequency of $f_1 = 25$ Hz. Moreover, at 360 µF, the highest current load of the capacitors is observed at $f_1 = 45$ Hz, and not at $f_1 = 50$ Hz, as in the other two cases. In all cases, there is a decreasing trend for k_{I4} with increasing frequency. But at 8360 µF k_{I4} increases slightly above 40 Hz, and at 2200 µF – above 45 Hz of fundamental frequency.

The fourth position regarding the occurrence of resonances of the SF capacitances with the AC grid side of the drive is impossible due to the one-way conductivity of the diodes of the input uncontrolled rectifier (6 pulse, bridge type) of the FC. As can be seen from Figure 7, I_C, consumed from the AC grid by the electric drive (current of the high-voltage winding of the step-down transformer) weakly depends on the presence and parameters of the SF. It should be noted that there is a slight increase of I_C in the presence of SF compared to its absence (by 1–41%, higher values correspond to a lower IM load). For the current consumed from the AC grid k_{IC} also varies somewhat depending on the SF capacity (Figure 9).

There is a possibility of resonance phenomena occurring between the inductive elements of the FC and the SF capacitors, as well as between the SF capacitors and the load inductances.

In [58], in paragraph 3.4 regarding the SF it is said: “The LC filter allows you to form a voltage waveform close to a sinusoidal one in the motor. In some cases, a dissipative element is added to the LC filter - a resistor, the inclusion of which eliminates the possibility of shock excitation processes occurring due to cyclic energy exchange in the “filter capacitance - motor inductance” circuit. In order to dampen possible resonant current oscillations in circuits containing SF capacitors, it was decided to connect resistors RA, RB, and RC in the capacitor power lines (Figure 1). Such technical solutions are used by electrical engineering companies, [59], [60]. Resistances of 0.013468 Ohms were selected, allowing for long-term dissipation of up to 8 kW per SF phase at continuous duty. Computer simulation has shown that it is possible to satisfy the limitation on power dissipation in resistors, taking into account the very complex harmonic composition of the currents through them, only with an SF phase capacitance of no more than 2360 µF. The temperature of the resistances during tests without blowing was 172 °C, which indicates the need for their forced cooling. Figure 10 shows the calculated energy characteristics of the SF with a capacity of 2200 µF per phase at $f_1 = 50$ Hz, $f_{car} = 2.5$ kHz, and $k_V = 32.3$ % for the linear voltage at the input of the SF. In the case of a f_{car} decrease, all other things being equal, the energy characteristics of the SF deteriorate.

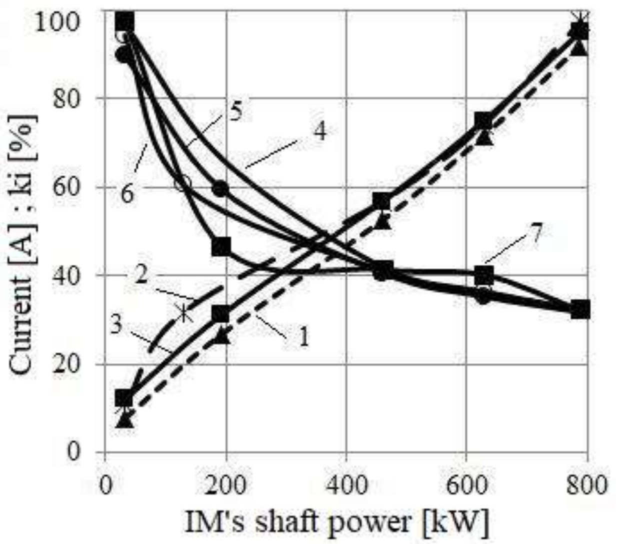

Fig. 9: Current consumed from the AC grid by the electric drive at $f_1 = 50$ Hz: 1 - I_C at $f_{car} = 2.5$ kHz, SF absence or in case a capacitance of 2200 µF per phase and damping resistors connected; 2 - I_C at $f_{car} = 2.5$ kHz, capacitance 8360 µF per SF phase without damping resistors; 3 - I_C at $f_{car} = 1$ kHz, capacitance 2200 µF per phase SF and damping resistors connected; 4 - k_{IC} at $f_{car} = 2.5$ kHz and SF absence; 5 - k_{IC} at $f_{car} = 1$ kHz, capacitance 2200 µF per phase and damping resistors connected; 6 - k_{IC} at $f_{car} = 2.5$ kHz, capacitance 8360 µF per phase without damping resistors; 7 - k_{IC} at $f_{car} = 2.5$ kHz, capacitance 2200 µF per phase and damping resistors connected

There is a possibility of resonance phenomena occurring between the inductive elements of the FC and the SF capacitors, as well as between the SF capacitors and the load inductances.

Figure 11 indicates the effectiveness of the influence of SF on the harmonic composition of the current. The largest parasitic current I_2 harmonic is the 5th.

According to Figure 10 and Figure 11, we can conclude that the SF characteristics are quite satisfactory at $f_1 = 50$ Hz and $f_{car} = 2.5$ kHz, excluding excessive specific current through the capacitance at low IM loads (Figure 6, Figure 7 and Figure 8). In other words, such an SF can be operated with a motor shaft power exceeding $0.4 \cdot P_{2rated}$. It is impossible to carry out commissioning work on a drive with such an SF without a load on the shaft or with a low load at continuous duty. It is quite possible to operate the SF in the entire range of IM loads at $f_1 < 49$ and $f_{car} = 2.5$ kHz. At $f_{car} = 1$ kHz, operation of the SF is impossible.

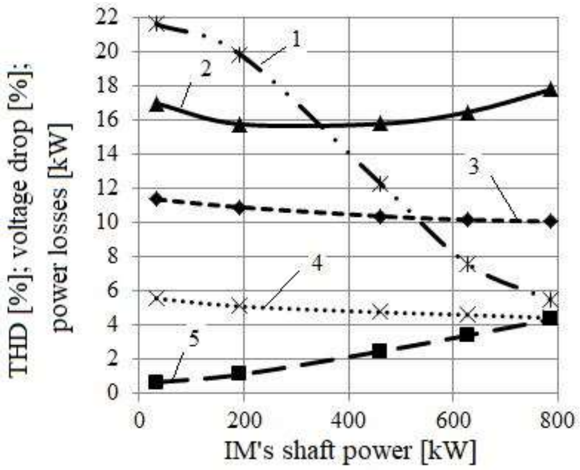

Fig. 10: Calculated energy characteristics of the SF: 1 - k_{I2}; 2 – SF's total losses; 3 - THD of phase-to-phase voltage at the load k_V; 4 – per phase power losses on the damping resistance; 5 – voltage drop from the fundamental harmonic in the SF phase

While allowing for reliable, trouble-free start of the drive, the introduction of damping resistors did not completely eliminate low-frequency current fluctuations (on the order of several hertz) at the inverter output at some output voltage frequencies. During tests with a SF capacitance of 2000 μF per phase, fluctuations in the effective current value were up to 17% of the average value at $f_1 = 50$ Hz and over 11% at $f_1 = 38$ Hz. An increase in current during acceleration is noted to approximately $f_1 = 30$ Hz. Above a frequency of 30 Hz, a decrease in I_1 current values followed. Since during the tests the rate of increase in frequency by the converter was set to 50 Hz for 90 s, the phenomena of the inrush current of the IM should have ended before reaching a frequency of 30 Hz.

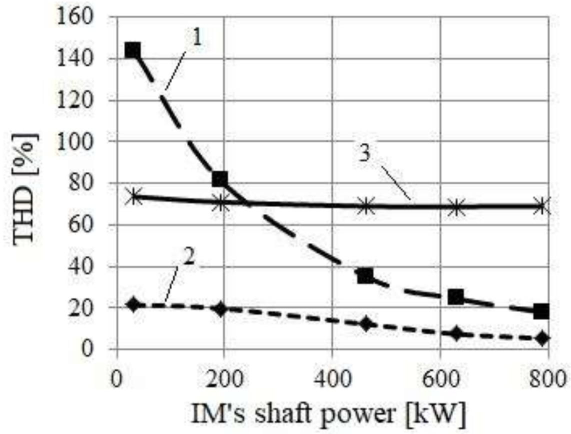

Fig. 11: Calculated THDs for SF currents: 1 - k_{I1}; 2 - k_{I2}; 3 - $k_{I3} = k_{I4}$

Therefore, it is possible that there are resonance phenomena in the amplitudes of the FC and IM currents. During the analysis of the results of computer simulation, it was noted that with the power of $0.05 \cdot P_{2rated}$ on the IM shaft at various values, there are fluctuations in the rotor speed with a frequency of approximately $f_{cr} = 5...7.25$ Hz (arithmetic mean 6.125 Hz). Their presence in the simulation results is not related to the size or absence of SF capacity. Under low load conditions, during oscillations of the rotor speed, periodic outputs of the IM into generator mode are possible. The amplitude of the IM phase current I_2 and the amplitude of the output current of the inverter I_1 have the same oscillation period. There are also fluctuations in the power released at the resistances of the reactors and damping resistors, the same frequency as the fluctuations in the rotation speed of the IM rotor. Power fluctuations are most noticeable at $f_1 = 25$ Hz and 35 Hz. Accordingly, the oscillation frequencies are about 5 Hz and 6.67 Hz. The same frequencies of amplitude oscillations are recorded in the results of modeling the drive network current. An increase in the mains current as a result of such fluctuations could explain the isolated cases of tripping of the step-down transformer protection recorded during testing. The frequency values of the inverter output voltage, for which an increase in I_1 amplitude was observed during testing and simulation, namely: 12 Hz, 25 Hz, 27 Hz, 35 Hz, 38 Hz, 42 Hz, 47 Hz, 50 Hz, are close to numbers that are multiples of f_{cr}.

In [61], it is indicated that for powerful IM powered by high-voltage FC, drives pumping unit, the occurrence of self-oscillations of current and rotation speed is possible. In other words, manifestations of I_1 current resonant phenomena are possible. There is no mention in [61] of the presence or absence of FC's output filters in the circuit. The main criterion for the propensity of the IM to enter resonance in [61] is the value of the magnetic flux transmission coefficient between the stator and the rotor $k \geq 0.95$

$$k = L_{\mu} / \sqrt{\left(L_{\mu} + L_{\sigma 1}\right)\left(L_{\mu} + L_2'\right)} \qquad (1)$$

For IM used on the WPS, the components of (1) have the values indicated in Table 1.

It is obvious that a particular IM meets the criterion of propensity to enter into resonance, since the calculated $k = 0.955 > 0.95$. It is possible that the presence of a capacitive energy storage device at the load terminals contributes to the aggravation of the manifestations of this tendency since no noticeable low-frequency I_1 current swings were recorded during tests when starting the drive without an SF.

The fifth position is reflected, for example, in [54], [62], where a correspondence is established between the rated power of the IM at 0.4 kV line voltage with a synchronous rotation speed of 1500 rpm and the maximum reactive power of compensating capacitors, kVAr, connected to the motor terminals, guaranteeing the absence of self-excitation of IM (Table 2 in Appendix). From Table 3 (Appendix) it follows that the capacitances of powerful SFs for operation at $f_{car} = 2$ kHz of known manufacturers [63], [64], [65] meet the requirements of Table 2 (Appendix). Low capacitance in the SF is achieved by increasing the inductance, which in some cases leads to a voltage drop across the inductance of more than 10%. However, [54], [62] do not deny the possibility of using capacitances larger than those recommended.

A possible compromise solution for using SF in a two-transformer circuit for powering a medium-voltage IM from a low-voltage inverter is to install medium-voltage capacitors [66] on the terminals of the high-voltage winding of a step-up transformer, the leakage inductance of which in this case serves as the inductance of the SF.

Table. 1 Values of the components of (1), [58]

Main inductance of the IM L_{μ}, H	Stator winding phase leakage inductance $L_{\sigma 1}$, H	Leakage inductance of the rotor squirrel cage reduced to the stator phase L_2', H	Magnetic flux transfer coefficient between stator and rotor k, p.u.
IM of rated shaft power 630 kW, synchronous speed 1500 rpm, rated linear RMS voltage 6 kV			
0.277214	0.01084367	0.01518114	0.955

The advantages of this solution: the capacitance of the SF is small and is formed by a single capacitor per phase, the recommendations of Table 2 (Appendix) are satisfied (if we assume that the maximum reactive power of capacitors that can be connected to the IM terminals without the risk of self-excitation does not depend on voltage). The disadvantage will be the lack of protection through the SF step-up transformer. For WPS, in some cases, this option is acceptable, since the phenomenon of ozonation needs to be eliminated in rooms where people are. IM with pumping units installed in the machine room where personnel work. Transformers are installed in separate boxes where public access is limited.

In the case under consideration with a medium-voltage IM with a power of 630 kW, medium-voltage capacitors KEK1-6.3-75, connected in a star configuration, can be used (Figure 12 in Appendix). The capacitor capacity is 6 µF. Each capacitor is connected to the rated phase voltage $V_{Cphrated} = 6300 / \sqrt{3} = 3467$ V. The rated current of the capacitor is calculated from the rated reactive power and rated voltage: $I_{Crated} = \frac{Q_{Crated}}{V_{Crated}} = \frac{75000}{6300} = 11.905$ A. The capacitor allows a current overload of 30%. At rated current and phase voltage, the reactive power of the three phases of the SF capacitors will be $Q_{C3ph} = 3V_{Cphrated} I_{Crated} = 3 \cdot 3467 \cdot 11.905 = $ $= 123823.9$ VAr, that is, 123.8 kVAr, which is slightly more than the limit value (123 kVAr) from the Table 2 (Appendix). The nature of the dependence of the current through the capacitor on the load on the IM shaft is the same as with low-voltage capacitors: at a constant voltage frequency, as the load increases, the current through the SF capacitors decreases. That is, the capacitor current for no load mode will be greatest. By simulating with the IM $0.05 \cdot P_{2rated}$ loaded, the RMS value of the current through the capacitor SF in a steady state is 11.439 A, which is lower than the rated current. RTST reactors in this case are practically not a significant part of the SF inductance - mainly its function is performed by the leakage inductances of the windings of the TSZGLF 1250/10 U3 transformer, used as a step-up, for which, in a first approximation, the sum of the leakage inductances of the windings is $L_{\sigma 1} + L_2' = 2 \cdot 0.0036 = 0.0072$ H.

Then $f_{car} / f_r = 2500 / 765.7 = 3.265$.

4 Conclusions

1. When using SF capacitances composed of parallel-connected capacitors with different characteristics, the smallest possible value of the specific RMS current through the capacitor should be taken as a current limit.
2. When using SF capacitors made up of a specific set of parallel-connected capacitors with different ratings, it should be possible for the consumer to use different combinations of capacitor ratings, allowing the SF capacitor to be adjusted for specific operating conditions. It should be possible to operate the SF both without and with damping resistors in the capacitive part.
3. SF capacitors are most loaded with current in case of the no-load mode of IM (or another load device). The SF must provide the ability to operate at continuous duty with real no-load mode, for example, IM, over the entire range of output voltage and frequency of the inverter. This is very important for commissioning work.
4. In the SF, you should not use a capacitance larger than that suitable to ensure full compensation of the reactive power of the load. Violation of this rule leads to an unjustified increase in the output current of the inverter and the current through the SF capacitors.
5. The method for calculating the RMS value of the current through the capacitance of the SF should ensure correct consideration of the contribution of a wide range of higher temporal harmonics. It is advisable to carry out a computer simulation of the steady-state operating modes of the drive to calculate the RMS value of the current through the capacitance, and dynamic modes to identify the maximum instantaneous current values. Calculation of the RMS value of the current through the SF capacitance using the method described in [67] (for example: Trace expression-> SQRT(S(I(R5)*I(R5))/Time), based on the results of the dynamic modes of the drive simulation, can lead to underestimated values if the long-range steady-state cycle has not been reached.
6. Reducing the specific RMS current through the SF capacitance by increasing the resistance of damping resistors is impractical. For example, a twofold increase in resistance leads to an increase in losses on it by 83% while the specific RMS current through the SF capacitance decreases by only 4%.
7. As a rule, capacitors of type “AC filtering” are suitable for composing the SF capacitance. The main characteristics for selection will be the voltage amplitude on the capacitor and the amplitude of the current through the capacitor. It is also necessary to take into account the RMS voltage across the capacitor and the RMS current through the capacitor. In order to prevent an overcurrent when choosing a capacitor, it is recommended that, having calculation or simulation result on the amplitude of the current through the capacitor, calculate the RMS value of the current from its amplitude as for a sinusoidal waveform, i.e. dividing the calculated amplitude value of the current through the capacitor by $\sqrt{2}$. The RMS value of the current through the capacitor obtained as a result of the calculation should be further used to select a capacitor from the catalog [68], [69], [70] if it also indicates the RMS value under the name Imax, acting on the principle “select a value from the catalog that is not less than the calculated one”. Maximum current $I_{\max}$ – the maximum permissible RMS value of the current through the capacitor in continuous operation, this value is usually given in the technical specifications, it determines the maximum power dissipated by the capacitor. Also, when choosing a capacitor, you can focus on the peak repeating current $\hat{I}$ - this is the permissible current amplitude in a repeating mode. The current $\hat{I}$ exceeds $I_{\max}$ from 3 to 40 and more times. For the selected capacitors, you should select a suitable protection device against overcurrents and overload currents.

References:

[1] M.Y. Pustovetov, Voinash S.A., "Analysis of dv/dt Filter Parameters Influence on its Characteristics. Filter Simulation Features," *2019 International Conference on Industrial Engineering, Applications and Manufacturing (ICIEAM)*, Sochi, Russia, 2019, pp. 1-5, https://doi.org/10.1109/ICIEAM.2019.8743007.

[2] Pastura M., Nuzzo S., Kohler M., Barater D., "Dv/Dt Filtering Techniques for Electric Drives: Review and Challenges," *IECON 2019 - 45th Annual Conference of the IEEE Industrial Electronics Society*, Lisbon, Portugal, 2019, pp. 7088-7093, https://doi.org/10.1109/IECON.2019.8926663.

[3] Haider M., Niklaus P.S., Madlener M., Rohner G., Kolar J.W., Comparative Evaluation of Gate Driver and LC-Filter Based dv/dt-Limitation for SiC-Based Motor-Integrated Variable Speed Drive Inverters, *IEEE Open Journal of Power Electronics*, Vol. 4, 2023, pp. 450-462. https://doi.org/10.1109/OJPEL.2023.3283052.

[4] Pontt J., Rodriguez J., Kouro S., Silva C., Farias H., Rotella M., "Output sinus filter for medium voltage drive with direct torque control," *Fourtieth IAS Annual Meeting. Conference Record of the 2005 Industry Applications Conference*, Hong Kong, China, 2005, pp. 204-209 Vol. 1, https://doi.org/10.1109/IAS.2005.1518311.

[5] Arhin B., Cha H., "A New dv/dt Filter Design Method using the Voltage Reflection Theory," *2022 4th Global Power, Energy and Communication Conference (GPECOM)*, Nevsehir, Turkey, 2022, pp. 107-111, https://doi.org/10.1109/GPECOM55404.2022.9815657.

[6] Anirudh Acharya B., John V., "Design of output dv/dt filter for motor drives," *2010 5th International Conference on Industrial and Information Systems*, Mangalore, India, 2010, pp. 562-567, https://doi.org/10.1109/ICIINFS.2010.5578641

[7] Mart-ro P., Sae-Kok W., Khomfoi S., "Analysis of dv/dt filter installation for PWM AC drive applications," *2011 IEEE Ninth International Conference on Power Electronics and Drive Systems*, Singapore, 2011, pp. 177-184, https://doi.org/10.1109/PEDS.2011.6147243.

[8] *Baek S., C*hoi D., Bu H., Cho Y., Analysis and Design of a Sine Wave Filter for GaN-Based Low-Voltage Variable Frequency Drives, *Electronics*, Vol. 9, No. 345, 2020, pp. 1-12. https://doi.org/10.3390/electronics9020345.

[9] Dresvianskii E., Pokushko M., Stupina A., Panteleev V., Yurdanova V., Control of high-voltage pump motor using a frequency sine-wave filter converter, *IOP Conference Series: Materials Science and Engineering*, Vol. 450, Iss. 7, No. 072003, 2018, pp. 1-6. https://doi.org/10.1088/1757-899X/450/7/072003.

[10] Petrov V.L., Pichuev A.V., Assessing the efficiency of measures to enhance electric power quality in variable-frequency drive for scraper conveyors, *Mining Science and Technology (Gornye nauki i tekhnologii)*, Vol. 9 (1), 2024, pp. 60-69. https://doi.org/10.17073/2500-0632-2024-01-198.

[11] Marignetti F., Rubino G., Boukadida Y., Conti P., De Gregorio F., Iengo E., Longobardi V.G., "Noise and vibration analysis of an inverter-fed three-phase induction motor," *2020 International Symposium on Power Electronics, Electrical Drives, Automation and Motion (SPEEDAM)*, Sorrento, Italy, 2020, pp. 157-161, https://doi.org/10.1109/SPEEDAM48782.2020.9161859.

[12] Belmans R.J.M., Noise in Inverter-Fed Squirrel-Cage Induction Motors. In: Ertan, H.B., Üçtuğ, M.Y., Colyer, R., Consoli, A. (eds) *Modern Electrical Drives*. NATO ASI Series, Vol. 369. Springer, Dordrecht, 2000. https://doi.org/10.1007/978-94-015-9387-8_26.

[13] Delgado-Arredondo P.A., Romero-Troncoso R.J., Duque-Pérez O., Morinigo-Sotelo D., Osornio-Rios R.A., "Vibration, Acoustic Noise Generation and Power Quality in Inverter-fed Induction Motors," *2019 IEEE 12th International Symposium on Diagnostics for Electrical Machines, Power Electronics and Drives (SDEMPED)*, Toulouse, France, 2019, pp. 412-418, https://doi.org/10.1109/DEMPED.2019.8864844.

[14] Hughes A., Drury B., Chapter Eight - Inverter-fed Induction Motor Drives, Editors: Austin Hughes, Bill Drury, *Electric Motors and Drives (Fourth Edition*), Newnes, 2013, pp. 255-279, https://doi.org/10.1016/B978-0-08-098332-5.00008-5.

[15] Tsikhalevsky I., Vakhrushev K., Rusakov A., "Analysis of the causes of failures of TED bearings of Lastochka electric trains," *AIP Conf. Proc.*, Vol. 2624, No. 020032, 2023. https://doi.org/10.1063/5.0132813.

[16] Ma J., Xue Y., Han Q., Li X., Yu C.. Motor Bearing Damage Induced by Bearing Current: A Review, *Machines*, Vol. 10 (12), No. 1167, 2022, pp. 1-23. https://doi.org/10.3390/machines10121167.

[17] Sundaresan A., Chandorkar M., "Traction Motor Bearing Failures Due to Bearing Currents in Electric Locomotives," *2019 IEEE Transportation Electrification Conference and Expo (ITEC)*, Detroit, MI, USA, 2019, pp. 1-6, https://doi.org/10.1109/ITEC.2019.8790569.

[18] Vostrov K., Pyrhönen J., Ahola J., "Shielding the end windings to reduce bearing currents," *2020 International Conference on Electrical Machines (ICEM)*, Gothenburg, Sweden, 2020, pp. 1431-1437, https://doi.org/10.1109/ICEM49940.2020.9270673.

[19] Zelentsov V., Ippolitov V., Dyshlevoy I., "A technique analysis of ways to compensate high-frequency currents on traction electric machines mechanical units," *2021 XVIII International Scientific Technical Conference Alternating Current Electric Drives (ACED)*, Ekaterinburg, Russia, 2021, pp. 1-4, https://doi.org/10.1109/ACED50605.2021.9462315.

[20] Zheng J., Xiang D., Li H., Quach D.-C., "An Investigation into the Effect of Bearing Grease Degradation on the High-frequency dv/dt Bearing Current in an Inverter-fed Motor System," *2021 6th International Conference on Power and Renewable Energy (ICPRE)*, Shanghai, China, 2021, pp. 543-547, https://doi.org/10.1109/ICPRE52634.2021.9635227.

[21] Alvarez-Gonzalez F., Hewitt D., Griffo A., Wang J., Diab M., Yuan X., "Design of Experiments for Stator Windings Insulation Degradation under High dv/dt and High Switching Frequency," *2020 IEEE Energy Conversion Congress and Exposition (ECCE)*, Detroit, MI, USA, 2020, pp. 789-795, https://doi.org/10.1109/ECCE44975.2020.9235940.

[22] Petrarca C., Egiziano L., Tucci V., Vitelli M., "Investigation on performances of insulation materials for inverter-fed traction motors," *1998 Annual Report Conference on Electrical Insulation and Dielectric Phenomena (Cat. No.98CH36257)*, Vol. 2, Atlanta, GA, USA, 1998, pp. 564-567, https://doi.org/10.1109/CEIDP.1998.732960.

[23] Saeed M., Fernández D., Guerrero J.M., Díaz I., Briz F., Insulation Condition Assessment in Inverter-Fed Motors Using the High-Frequency Common Mode Current: A Case Study. *Energies*, Vol. 17 (2), No. 470, 2024, pp. 1-16, https://doi.org/10.3390/en17020470.

[24] Ozone: Health hazards and control measures. Guidance Note EH38, [Online]. https://www.hse.gov.uk/pubns/eh38.pdf (Accessed Date: June 23, 2024).

[25] Dmitriev V., Oliveira R.M.S., Zampolo R.F., Moutinho de Vilhena P.R., de Souza Brasil F., Fernandes M.F., Partial Discharges and Ozone. In: *Partial Discharges in Hydroelectric Generators. Power Systems*. Springer, Cham., 2024. https://doi.org/10.1007/978-3-031-36604-8_7.

[26] European Standard UNE EN 50160:2023. *Voltage characteristics of electricity supplied by public electricity networks*, [Online]. https://cdn.standards.iteh.ai/samples/71003/490b981fbec343edb9db83f8ce4b2b3d/SIST-EN-50160-2023.pdf (Accessed Date: October 21, 2024).

[27] Holmes D.G., Lipo T.A., *Pulse width modulation for power converters: principles and practice*, Hoboken, NJ: John Wiley, 2003, [Online]. https://ieeexplore.ieee.org/book/5264450 (Accessed Date: October 21, 2024).

[28] State Standard GOST R 54149-2010. *Electric energy. Electromagnetic compatibility of technical equipment. Standards for the quality of electrical energy in general-purpose power supply systems*, Moscow, Russia: Standartinform, 2012, [Online]. https://files.stroyinf.ru/Data/524/52435.pdf?ysclid=m2iwtsqvmu547869952 (Accessed Date: October 21, 2024).

[29] Jones G.M., Bosserman II B.E., Sanks R.L., Tchobanoglous G., *Pumping Station Design, 3d edition*, Butterworth-Heinemann, 2006, [Online]. https://vdoc.pub/download/pumping-station-design-third-edition-od4s9sn73ps0 (Accessed Date: October 11, 2024).

[30] Pustovetov M., Shukhmin K., Goolak S., Matijošius J., Kravchenko K., *Induction Motor Computer Models in Three-Phase Stator Reference Frames: A Technical Handbook*, Bentham Science Publishers Pte. Ltd. Singapore, 2023. https://doi.org/10.2174/97898151243091230101

[31] H. Mahdi, B. Hoff, T. Østrem, A Review of Power Converters for Ships Electrification, *IEEE Transactions on Power Electronics*, Vol. 38, No. 4, pp. 4680-4697, 2023, https://doi.org/10.1109/TPEL.2022.3227398.

[32] Bin Wu, Mehdi Narimani, *High-Power Converters and AC Drives, 2nd edition*, Wiley-IEEE Press, 2017. https://doi.org/10.1002/9781119156079.

[33] Standard IEC 60034-1:2022. *Rotating electrical machines - Part 1: Rating and performance*, [Online]. https://webstore.iec.ch/en/publication/65446 (Accessed Date: October 11, 2024).

[34] Parisher R.A., Rhea R. A.. *Pipe Drafting and Design. Fourth Edition*, Gulf Professional Publishing, 2021. https://doi.org/10.1016/C2019-0-01022-9.

[35] Chicco D., Warrens M.J., Jurman G., The coefficient of determination R-squared is more informative than SMAPE, MAE, MAPE, MSE and RMSE in regression analysis evaluation, *PeerJ Computer Science*, Vol. 7, No. e623, 2021. https://doi.org/10.7717/peerj-cs.623.

[36] Kvalseth T.O., Cautionary Note about R^2, The American Statistician, Vol. 39, No. 4, Part 1, Nov., 1985, pp. 279-285. https://doi.org/10.2307/2683704.

[37] Keown J, *OrCAD PSpice and Circuit Analysis*, *4th edition*, Prentice Hall, 2000.

[38] Rashid M.H., *SPICE for Power Electronics and Electric Power*, *3rd edition*, Boca Raton, USA: CRC Press, 2012. https://doi.org/10.1201/b12105.

[39] Fitzpatrick D., *Analog Design and Simulation Using OrCAD Capture and PSpice, 2nd edition*, Newnes, 2017.

[40] Pustovetov M., Determining the Parameters of the Sine-Wave Filter. Factors Affecting Filtration Quality. *Journal of Engineering Research and Sciences*, Vol.1, No.4, 2022, pp.127-136. https://doi.org/10.55708/js0104015.

[41] Niu Yanshu, "Single Phase Sine Wave PWM Inverter Circuit Simulation and the Design of Filter Based on Matlab," *2018 2nd International Conference on Electronic Information Technology and Computer Engineering (EITCE 2018)*, MATEC Web Conf., Vol. 232, No. 04030, 2018, pp. 1-4, https://doi.org/10.1051/matecconf/201823204030.

[42] Nerubatskyi V., Plakhtii O., Hordiienko D., Mykhalkiv S., Ravluyk V., A Method for Calculating the Parameters of the Sine Filter of the Frequency Converter, Taking into Account the Criterion of Starting Current Limitation and Pulse-Width Modulation Frequency, *Eastern-European Journal of Enterprise Technologies (EEJET)*, No. 1 (8 (109)), 2021, pp. 6-16, https://doi.org/10.15587/1729-4061.2021.225327.

[43] Ansari M.I., Misra H., "Impact of Sine-Wave LC filter on Two-Level PWM VSI fed IM drive considering the long leads," *2020 21st National Power Systems Conference (NPSC)*, Gandhinagar, India, 2020, pp. 1-6, https://doi.org/10.1109/NPSC49263.2020.9331949.

[44] Vdovin V.V., Kotin D.A., Pankratov V.V., "Parameters determination in the sine filters for AFE converters and VSI with PWM," *2014 15th International Conference of Young Specialists on Micro/Nanotechnologies and Electron Devices (EDM),* Novosibirsk, Russia, 2014, pp. 383-386, https://doi.org/10.1109/EDM.2014.6882553.

[45] Zehelein M., Fischer M., Nitzsche M., Roth-Stielow J., "Influence of the Filter Design on Wide-Bandgap Voltage Source Inverters with Sine Wave Filter for Electrical Drives," *2019 21st European Conference on Power Electronics and Applications (EPE '19 ECCE Europe)*, Genova, Italy, 2019, pp. 1-10, https://doi.org/10.23919/EPE.2019.8914968.

[46] Cacciato M., Scarcella G., Scelba G., Pecoraro G., "Genetic algorithms based design technique of sine wave filters for AC motor drives," *2014 ELEKTRO*, Rajecke Teplice, Slovakia, 2014, pp. 208-213, https://doi.org/10.1109/ELEKTRO.2014.6847902.

[47] Pustovetov M.Y., "A mathematical model of the three-phase induction motor in three-phase stator reference frame describing electromagnetic and electromechanical processes," *2016 Dynamics of Systems, Mechanisms and Machines (Dynamics)*, Omsk, Russia, 2016, pp. 1-5, https://doi.org/10.1109/Dynamics.2016.7819069.

[48] Goolak S., Liubarskyi B., Sapronova S., Tkachenko V., Riabov Ie. "Refined model of asynchronous traction electric motor of electric locomotive," *The proceedings of the 25th International Scientific Conference Transport Means 2021 - Sustainability: Research and Solutions, Part I*, Kaunas, Lithuania, 2021, pp. 455-460, [Online]. https://transportmeans.ktu.edu/wp-content/uploads/sites/307/2018/02/Transport-Means-2021-Part-I.pdf (Accessed Date: June 23, 2024).

[49] Goolak S., Gorobchenko O., Nezlina O., Riabov I., Yurchenko V., Improvement of the model of an asynchronous traction motor of an electric locomotive by taking into account power losses, *Przeglad Elektrotechniczny*, Vol. 98, No. 5, 2022, pp. 1-10. https://doi.org/10.15199/48.2022.05.01.

[50] Goolak S., Liubarskyi B., Sapronova S., Tkachenko V., Riabov I., Glebova M., Improving a model of the induction traction motor operation involving non-symmetric stator windings, *Eastern-European Journal of Enterprise Technologies*, Vol. 4, No. 8-112, 2021, pp. 45-58. https://doi.org/10.15587/1729-4061.2021.236825.

[51] Pustovetov M.Y., A universal mathematical model of a three-phase transformer with a single magnetic core, Russian Electrical Engineering, Vol. 86, 2015, pp. 98–101. https://doi.org/10.3103/S106837121502011X.

[52] Kabalyk I., Gutsol A., "Simulation of control and measurement systems for dc-ac inverter," *International Scientific Conference Topical Problems of Architecture, Civil Engineering and Environmental Economics (TPACEE-2018)*, E3S Web of Conferences., Vol. 91, No. 01008, 2019, pp. 1-8. https://doi.org/10.1051/e3sconf/20199101008.

[53] Juromskiy V.M., Engineering model of the electric drives of separation device for simulation of automatic control systems of reactive power compensation by means of serially connected capacitors, *Journal of Physics: Conference Series*, Vol. 751, No. 012010, 2016. https://doi.org/ 10.1088/1742-6596/751/1/012010.

[54] Electrical installation guide. According to IEC international standards. Schneider Electric, [Online]. https://download.schneider-electric.com/files?p_enDocType=Technical+leaflet&p_File_Name=Electrical+Installation+Guide+2018.pdf&p_Doc_Ref=EIGED306001EN (Accessed Date: June 23, 2024).

[55] Fazal M, Waleed Raza M, Khan S, Faizullah, Reactive Power Compensation by Power Capacitor Method, *Engineering Technology Open Access Journal*, Vol. 1 (3), No. 555565, 2018, pp. 0092-0095. https://doi.org/10.19080/ETOAJ.2018.01.555565.

[56] Kazakbaev V., Oshurbekov S., Prakht V., Dmitrievskii V., Feasibility Study of Direct-on-Line Energy-Efficient Motors in a Pumping Unit, Considering Reactive Power Compensation, Mathematics, Vol. 9, No. 2196, 2021, pp. 2-14. http://doi.org/10.3390/math9182196.

[57] EATON. December 2015. Sheet 35001. Power Factor Capacitors and Detuned Filters, [Online]. https://www.eaton.com/content/dam/eaton/products/design-guides---consultant-audience/canada/cag/eaton-power-factor-capacitors-detuned-filters-consulting-application-guide-tb02608001e-tab-35-ca08104001e-ca.pdf (Accessed Date: June 23, 2024).

[58] Khachaturyan V.A., *Control of power supply of oil refineries in conditions of mass use of adjustable electric drives*, St. Petersburg, Russia: Publishing house of Peter the Great St.Petersburg Polytechnic University, 2001.

[59] Cacciato M., Scarcella G., Scelba G., Spanik P., Sine Wave Filters Design for AC Motor Drives with Genetic Algorithms, Communications - Scientific Letters of the University of Zilina, Vol. 17(1A), 2015, pp. 102-109. https://doi.org/10.26552/com.C.2015.1A.102-109.

[60] MotorGuard KMG High Performance Output Sine Wave Filter. Installation, Operation, and Maintenance Manual. TCI, [Online]. https://files.valinonline.com/userfiles/documents/tci-kmg-user-manual.pdf (Accessed Date: June 23, 2024).

[61] Chepkunov R.A., Study of electromechanical self-oscillations in an induction motor based electric drive at low frequencies, *Bulletin of Kremenchug National University named after Mikhail Ostrogradsky*, No. 4/2008 (51), Part 2, 2008, pp. 17-20.

[62] EMC Filters, [Online]. https://file.elecfans.com/web1/M00/20/D5/oYYBAFmk2Q-ACM1GAIIw7rko1CM261.pdf (Accessed Date: June 23, 2024).

[63] Danfoss. Output Filters Design Guide, [Online]. https://www.rpmecatronica.com/system/storage/download/130B2447.pdf?key=GG48eKtcD68412CiJv4wXIE4dD8zpzLZ (Accessed Date: June 23, 2024).

[64] Data Sheet. Sine Wave Filters FN5040HV. Schaffner, [Online]. https://www.schaffner.com/product/FN5040HV/Schaffner_datasheet_FN5040HV.pdf (Accessed Date: June 23, 2024).

[65] Data Sheet. Sine Wave Filters FN5420. Schaffner, [Online].

https://www.schaffner.com/product/FN5420/Schaffner_datasheet_FN5420.pdf (Accessed Date: June 23, 2024).

[66] Reactive Power Compensation of High Voltage Power System, [Online]. https://tdneoteh.ru/files/20161215-104221_516792895.pdf (Accessed Date: June 23, 2024).

[67] Bolotovskii Yu.I., Tanazly G.I., *OrCAD. Modelirovanie "Povarennaya kniga" (OrCAD. "Cookbook" for Simulation)*, Moscow, Russia: Solon-press, 2005.

[68] Power Electronics Capacitors, [Online]. https://www.nucon.ru/upload/iblock/b42/DC-2016.pdf (Accessed Date: June 23, 2024).

[69] Electronic Power Capacitors. EPC Series. RTR Energia, [Online]. https://rtrenergia.es/wp-content/uploads/2023/03/AC-FILTERING-.pdf (Accessed Date: June 23, 2024).

[70] AC Filter Capacitors, [Online]. https://www.zez-silko.com/data/uploadHTML/files/download-pe-power-electronics/ac-filter-capacitors.pdf (Accessed Date: June 23, 2024).

Contribution of Individual Authors to the Creation of a Scientific Article (Ghostwriting Policy)

The author equally contributed to the present research, at all stages from the formulation of the problem to the final findings and solution.

Sources of Funding for Research Presented in a Scientific Article or Scientific Article Itself

No funding was received for conducting this study.

Conflict of Interest

The author has no conflicts of interest to declare that are relevant to the content of this article.

APPENDIX

Table 2. Recommended correspondence between the rated power of the IM and the maximum reactive power of the capacitors

Rated power of the IM, kW	Maximum reactive power of capacitors, kVAr	C, μF (per phase) when connected according to a delta circuit for a RMS voltage of 0.4 kV
22	8	53
30	10	66
37	11	73
45	13	86
55	17	113
75	22	146
90	25	166
110	29	192
132	36	239
160	41	272
200	47	312
250	57	378
280	63	418
355	76	504
400	82	544
450	93	617
	Subsequent values are obtained by extrapolation	
500	102	675
630	123	816
800	150	994

Table. 3. Characteristics of powerful SF in accordance with [63], [64], [65] for an RMS linear voltage of 0.4 kV

Rated power of the IM, kW	C, μF (per phase) when connected according to a delta circuit	L, mH	Resonant frequency of SF f_r, Hz	Carrier frequency of PWM inverter f_{car}, Hz	$\frac{f_{car}}{f_r}$	Voltage drop at a frequency of 50 Hz across the SF inductance in % of 380 V	Inverter output current, A
250	94	0.11	903.6	3000	3.3	4.4	480
400	165	0.2	505.8	2000	4.0	12.4	750
450	188	0.11	639.0	2000	3.1	8.0	880
500	188	0.11	639.0	2000	3.1	8.0	880
560	282	0.075	631.8	2000	3.2	7.4	1200
630	282	0.075	631.8	2000	3.2	7.4	1200
800	330	0.1	505.8	2000	4.0	12.4	1500

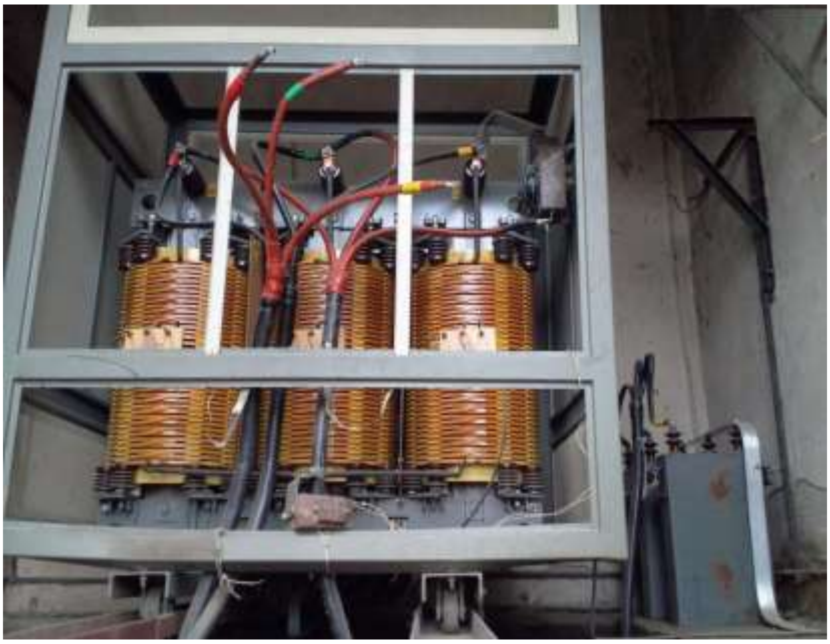

Fig. 12: Dry step-up power transformer 0.4/6 kV TSZ-1250/6/0.4 Y/Δ in an individual box. At the bottom right you can see medium-voltage cosine capacitors KEK1-6.3-75 to 6.3 kV, 75 kVAr, connected according to the Y circuit, acting as capacitive elements of the SF